Available online at www.sciencedirect.com
ScienceDirect
Pattern Recognition 41 (2008) 1316–1328
PATTERN RECOGNITION
THE JOURNAL OF THE PATTERN RECOGNITION SOCIETY
www.elsevier.com/locate/pr

Palmprint verification based on principal lines

De-Shuang Huang[a,*], Wei Jia[a,b], David Zhang[c]

[a]*Intelligent Computation Laboratory, Hefei Institute of Intelligent Machines, Chinese Academy of Science, P.O. Box 1130, Hefei, Anhui 230031, China*
[b]*Department of Automation, University of Science and Technology of China, Hefei 230027, China*
[c]*Biometrics Research Centre, Department of Computing, The Hong Kong Polytechnic University, Hong Kong*

Received 25 June 2006; received in revised form 22 August 2007; accepted 29 August 2007

Abstract

In this paper, we propose a novel palmprint verification approach based on principal lines. In feature extraction stage, the modified finite Radon transform is proposed, which can extract principal lines effectively and efficiently even in the case that the palmprint images contain many long and strong wrinkles. In matching stage, a matching algorithm based on pixel-to-area comparison is devised to calculate the similarity between two palmprints, which has shown good robustness for slight rotations and translations of palmprints. The experimental results for the verification on Hong Kong Polytechnic University Palmprint Database show that the discriminability of principal lines is also strong.

Keywords: Palmprint; Biometrics; Principal lines; Line detection; Modified finite Radon transform

1. Introduction

In networked society, automatic personal verification is a crucial problem that needs to be solved properly. And in this field biometrics is one of the most important and effective solutions. Recently, palmprint based verification systems (PVS) have been receiving more attention from researchers [1]. Compared with fingerprint or iris based personal verification systems which have been widely used [2,3], the PVS can also achieve satisfying performance. For example, it can provide reliable recognition rate with fast processing speed [1]. Particularly, the PVS has several special advantages such as rich texture feature, stable line feature, low-resolution imaging, low-cost capturing devices, and easy self-positioning, etc.

So far, there have been many approaches proposed for palmprint verification/identification, which can be mainly divided into five categories: (1) texture based approaches [1,4]; (2) appearance based approaches [5–8]; (3) multiple features based approaches [9]; (4) orientation based approaches [10,11]; and (5) line based approaches [12–18]. The main approaches based on texture are to extract texture feature by exploiting 2-D Gabor filter, which have been shown to be of satisfying performance in terms of recognition rate and processing speed [1,4]. Appearance based approaches were also reported to achieve exciting results in many literatures, but they may be sensitive to illumination, contrast, and position changes in real applications. In addition, it was reported in Ref. [9] that multiple features based approaches using information fusion technology could provide more reliable results. Recently, orientation codes are deemed to be the most promising methods, since the orientation feature contains more discriminative power than other features, and is more robust for the change of illumination.

Obviously, line is the basic feature of palmprint. Thus, line based approaches also play an important role in palmprint verification/identification field. Zhang et al. used overcomplete wavelet expansion and directional context modeling technique to extract principal lines-like features [12]. Han et al. proposed using Sobel and morphological operations to extract the line-like features from palmprint images obtained using a scanner [13]. Lin et al. applied the hierarchical decomposition mechanism to extract principal palmprint features from a region of interest (ROI), which includes directional and multi-resolution decompositions [14]. However, these methods cannot extract

* Corresponding author.
E-mail addresses: dshuang@iim.ac.cn (D.-S. Huang), jiawei78@mail.ustc.edu.cn (W. Jia), csdzhang@comp.polyu.edu.hk (D. Zhang).

0031-3203/$30.00 © 2007 Elsevier Ltd. All rights reserved.
doi:10.1016/j.patcog.2007.08.016

palm lines explicitly. Additionally, Wu et al. and Liu et al. proposed two different approaches based on palm lines, which will be discussed in later section [15–18].

It is well known that palm lines consist of wrinkles and principal lines. And principal lines can be treated as a separate feature to characterize a palm. Therefore, there are several reasons to carefully study principal lines based approaches. At first, principal lines based approaches can be jointly considered with the person's habit. For instance, when human beings are comparing two palmprints, they instinctively compare principal lines. Secondly, principal lines are generally more stable than wrinkles. The latter is easily masked by bad illumination condition, compression, and noise. Thirdly, principal lines can act as an important component in multiple features based approaches. Fourthly, in some special cases, for example, when the police is searching for some palmprints with similar principal lines, other features cannot be used to replace principal lines. At last, principal lines can be used in palmprint classification or fast retrieval schemes. However, principal lines based approaches have not been studied adequately so far. The main reason is that it is very difficult to extract principal lines from complex palmprint images, which contain many strong and long wrinkles. At the same time, many researchers claimed that it was difficult to obtain a high recognition rate using only principal lines because of their similarity among different people [1]. In other words, they thought the discriminability of principal lines was limited. Nevertheless, they did not conduct related experiments to verify their viewpoints.

In this paper, we propose a novel palmprint verification approach based on principal lines, and further discuss the discriminability of principal lines. Here, before presenting the proposed approach, we shall first present the definition of principal lines used in the whole paper. To illustrate this definition, three typical palmprint images are shown in Fig. 1. Generally speaking, most palmprints have three principal lines: heart line, head line, and life line, which are longest, strongest, and widest lines in palmprint image, and have stable line initials and positions (see Fig. 1(a)) [15]. In addition, a lot of palmprints may have more or less principal lines due to their diversity and complexity (see Fig. 1(b)). In this paper, assuming that within a few of palmprints one or two longest and strongest wrinkles that have similar directions to three principal lines are also regarded as a part of principal lines (see Fig. 1(c)).

In principal lines extraction stage, what are criterions for distinguishing principal lines from wrinkles is an important issue. Through careful observation and analysis, we adopt two main differences between principal lines and wrinkles as the corresponding criterions. The one is the line energy of which principal lines are stronger than that of wrinkles. Another one is the direction of which most wrinkles obviously differ from that of principal lines. In addition, since the Radon transform and its variations are powerful tools to detect the directions and energies of lines in an image, they are used in our method. In matching stage, we devise a matching algorithm based on pixel-to-area comparison to calculate the similarity between two palmprints, which have shown good robustness for slight rotations and translations.

Additionally, what we must stress here is that in this paper, all palmprint images are obtained from Hong Kong Polytechnic University Palmprint Database [19], which were captured by a CCD-based device described in Ref. [1]. This paper is organized as follows. Section 2 presents the method of principal line extraction. Section 3 gives the palmprint matching method based on pixel-to-area comparison. Section 4 reports the experimental results including principal lines extraction, verification, and computational time. Section 5 discusses the discriminability of principal lines. And Section 6 concludes the whole paper with some conclusive remarks.

2. Feature extraction based on the modified finite Radon transform

2.1. The Radon transform and the finite Radon transform

The Radon transform in Euclidean space was first established by Johann Radon in 1917 [20]. The Radon transform of a 2D function $f(x, y)$ is defined as

$$R(r, \theta)[f(x, y)] = \int_{-\infty}^{\infty}\int_{-\infty}^{\infty} f(x, y)\delta(r - x\ \cos\ \theta - y\ \sin\ \theta)\,\mathrm{d}x\,\mathrm{d}y, \quad (1)$$

where r is the perpendicular distance of a line from the origin and θ is the angle between the line and the y-axis. The Radon transform accentuates linear features by integrating image intensity along all possible lines in an image, thus it can be used to detect linear trends in the image.

However, there are some drawbacks using the Radon transform for linear feature detection when the intensity integration is performed over the entire length of the image. For example, it cannot effectively detect line segments which are significantly shorter than the image dimensions, etc. In order to overcome these problems of Radon transform, Copeand et al. proposed a modified Radon transform scheme, i.e., Localized Radon transform, which is defined as follows:

$$R(r, \theta)[f(x, y)] = \int_{x_{\min}}^{x_{\max}}\int_{y_{\min}}^{y_{\max}} f(x, y)\delta(r - x\ \cos\ \theta - y\ \sin\ \theta)\,\mathrm{d}x\,\mathrm{d}y, \quad (2)$$

where parameters $x_{\max}$, $x_{\min}$, $y_{\max}$, and $y_{\min}$ define a local area to perform Radon transform [21].

The finite Radon transform (FRAT) is another way to perform Radon transform for finite length signals [22]. FRAT is generally defined as the summation of image pixels over a certain set of lines. Denoting $\{Z_p = 0, 1, \ldots, p-1\}$, where p is a prime number, the FRAT of real function $f[x, y]$ on the finite grid Z_p^2 is defined as

$$r_k[l] = FRAT_f(k, l) = \frac{1}{\sqrt{p}} \sum_{(i,j)\in L_{k,l}} f[i, j], \quad (3)$$

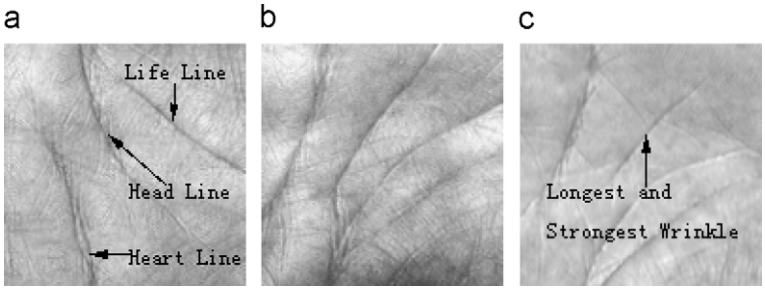

Fig. 1. Three typical palmprint images.

where $L_{k,l}$ denotes the set of points that make up a line on the lattice Z_p^2, which means:

$$L_{k,l} = \{(i, j) : j = ki + l (\mathrm{mod}\ p), i \in Z_p\}, \quad 0 \leqslant k < p,$$
$$L_{p,l} = \{(l, j) : j \in Z_p\}. \tag{4}$$

In Eq. (4), k represents the corresponding slope of the line and l represents the intercept.

2.2. Extracting principal lines using modified finite Radon transform

In a palmprint image, a palm line can be regarded as a straight line approximately in a small local area. Therefore, it can be detected by the FRAT. However, the FRAT treats the input image as a periodic image. Thus, these lines exhibit a "wrap around" effect due to the modulo operations in the definition of lines of the FRAT [23]. In order to eliminate this effect, we propose the modified finite Radon transform (MFRAT) to extract line feature of palmprint, which is defined as follows:

Denoting $Z_p = \{0, 1, \ldots, p-1\}$, where p is a positive integer, the MFRAT of real function $f[x, y]$ on the finite grid Z_p^2 *is defined as*

$$r[L_k] = MFRAT_f(k) = \frac{1}{C} \sum_{(i,j) \in L_k} f[i, j], \tag{5}$$

where C is a scalar to control the scale of $r[L_k]$, and L_k denotes the set of points that make up a line on the lattice Z_p^2, which means:

$$L_k = \{(i, j) : j = k(i - i_0) + j_0, i \in Z_p\}, \tag{6}$$

where (i_0, j_0) denotes the center point of the lattice Z_p^2, and k means the corresponding slope of L_k. In our paper, L_k has another expression $L(\theta_k)$, where θ_k is the angle corresponding to k.

Compared with the FRAT, the MFRAT removes the intercept l in $L_{k,l}$. Consequently, for any given slope k, the summation of only one line, which pass through the center point (i_0, j_0) of Z_p^2, is calculated. It should be pointed out that all lines at different directions have an identical number of pixels, and some pixels belonging to one line could lap over other lines. Unlike the FRAT, the number of k is not restricted by p, but determined by practical situation. In addition, the MFRAT is not an invertible transform. And note that before taking the MFRAT given in Eq. (5), the mean should be subtracted from an input f', thus we have:

$$f = f' - mean(f'), \tag{7}$$

$$\sum f[i, j] = 0 \quad (i, j) \in Z_p^2. \tag{8}$$

In the MFRAT, the direction θ_k and the energy e of center point $f(i_0, j_0)$ of the lattice Z_p^2 are calculated by the following formula:

$$\theta_{k_{(i_0,j_0)}} = \arg(\min_k(r[L_k])), \quad k = 1, 2, \ldots, N, \tag{9}$$

$$e_{(i_0,j_0)} = |\min(r[L_k])|, \quad k = 1, 2, \ldots, N, \tag{10}$$

where $|\cdot|$ denotes the absolute operation.

In this way, the directions and energies of all pixels are calculated if the center of lattice Z_p^2 move over an image pixel by pixel (or pixels by pixels). For an image $I(x, y)$ of size $m \times n$, if the values of all pixels are replaced by their directions and energies, two new images, *Direction_image* and *Energy_image*, can be created, respectively, i.e.

$$Direction\_image = \begin{vmatrix} \theta_{k(1,1)} & \theta_{k(1,2)} & \vdots & \theta_{k(1,n)} \\ \theta_{k(2,1)} & \theta_{k(2,2)} & \vdots & \theta_{k(2,n)} \\ \cdots & \cdots & \cdots & \cdots \\ \theta_{k(m,1)} & \theta_{k(m,2)} & \vdots & \theta_{k(m,n)} \end{vmatrix},$$

$$Energy\_image = \begin{vmatrix} e_{(1,1)} & e_{(1,2)} & \vdots & e_{(1,n)} \\ e_{(2,1)} & e_{(2,2)} & \vdots & e_{(2,n)} \\ \cdots & \cdots & \cdots & \cdots \\ e_{(m,1)} & e_{(m,2)} & \vdots & e_{(m,n)} \end{vmatrix}.$$

Fig. 2 shows two examples of the MFRAT whose sizes are 7×7 and 14×14, respectively, and whose lines, $L(\theta_k)$, are at directions of $\pi/12$, $2\pi/12$, …, and $6\pi/12$, respectively. Due to space limitation, the remaining lines $L(\theta_k)$ at directions of $7\pi/12$, $8\pi/12$, …, and $12\pi/12$, are not depicted here. If the line in the MFRAT is 1 pixel wide, p should be an odd number in order to clearly define the center of Z_p^2. In 14×14 MFRAT, the center area of Z_p^2 contains four pixels, thus the directions and the energies of these four pixels could be calculated

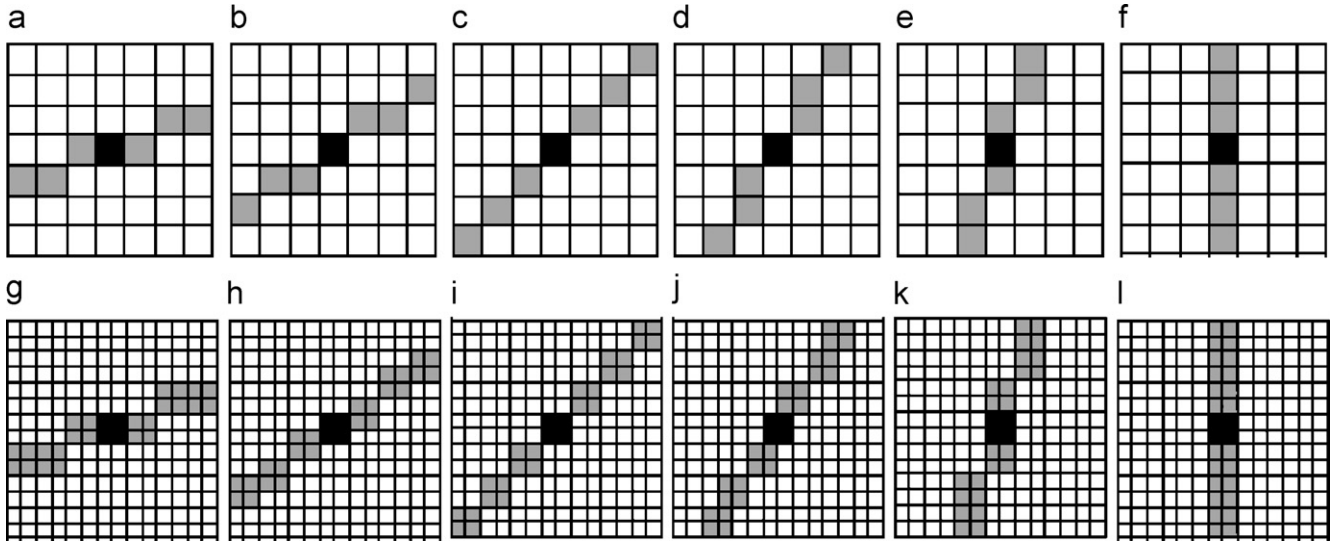

Fig. 2. The 7×7 and the 14×14 MFRAT. (a) and (g) $\theta_1 = \pi/12$; (b) and (h) $\theta_2 = 2\pi/12$; (c) and (i) $\theta_3 = 3\pi/12$; (d) and (j) $\theta_4 = 4\pi/12$; (e) and (k) $\theta_5 = 5\pi/12$; (f) and (l) $\theta_6 = 6\pi/12$.

simultaneously. After principal lines extraction, these four pixels, which have the same directions and energies, are regarded as one pixel. Thus, the size of feature image is resized to half of original image, which can be regarded as a subsampling operation. In the following example, the 14×14 MFRAT is performed on one 128×128 palmprint image. However, in order to demonstrate the processing clearly, the 128×128 feature image is presented instead of the 64×64 image.

Fig. 3 shows an example of principal lines extraction, which contains some images appearing in this stage. Fig. 3(b) is the *Energy_image* obtained from the original image of Fig. 3(a). It can be seen that the energies of all palm lines are extracted clearly and accurately. In Fig. 3(c), the important lines including principal lines and some strong wrinkles are extracted according to a threshold T. Here, the obtained binary image is called as *Lines_image*, which can be defined as

$$Lines\_image(x, y) = \begin{cases} 0 & \text{if Energy\_image}(x, y) < T, \\ 1 & \text{if Energy\_image}(x, y) \geqslant T. \end{cases} \quad (11)$$

In this step, many wrinkles are removed under the energy criterion. It should be pointed out that T is an important parameter here. We sort all pixel values of *Energy_image* in descending order, and select the Mth largest pixel value as its adaptive threshold T. In the above example, M was set to 1000.

Obviously, *Lines_image* also contains a lot of strong wrinkles. We can further remove them according to the direction criterion. Generally speaking, the directions of most wrinkles markedly differ from that of the principal lines. For instance, if the directions of principal lines belong to $(0°, \ldots, \frac{\pi}{2}]$ approximately, the directions of most wrinkles will be at $[\frac{\pi}{2}, \ldots, \pi)$ approximately, and vice versa. Under this prior knowledge, *Lines_image* is divided into *LA_image* (see Fig. 3(d)) and *LB_image* (see Fig. 3(e)) according to $\theta_{(x,y)}$ of every pixel. It should be noted that those points whose directions are $\pi/2$ are assigned to both *LA_image* and *LB_image,* i.e.:

$$\begin{aligned} LA\_image(x, y) = 1 \quad & \text{if } line\_image(x, y) = 1, \\ & \text{and } 0° < \theta_{(x,y)} \leqslant \pi/2, \\ LB\_image(x, y) = 1 \quad & \text{if } line\_image(x, y) = 1, \\ & \text{and } \pi/2 \leqslant \theta_{(x,y)} < \pi. \end{aligned} \quad (12)$$

For *LA_image* and *LB_image*, which one contains principal lines? Using Eq. (1), Radon transform is respectively performed on *LA_image* from 0 to $\pi/2$, and on *LB_image* from $\pi/2$ to π. Thus two Radon energy maps are created, which are $R[LA\_image(x, y)]$ (see Fig. 3(f)) and $R[LB\_image(x, y)]$ (see Fig. 3(g)). The transform can be implemented very fast since the images are at binary versions. As we know, the principal lines are generally longer and straighter than the wrinkles. Thus the Radon transform energy of principal lines will be greater than that of the wrinkles. For a binary image $F(x, y)$, there are two criterions that can be adopted to evaluate the Radon transform energy of $R[F(x, y)]$, i.e.:

$$E_{\max}(F(x, y)) = \max(R[F(x, y)]), \quad (13)$$

$$E_{total}(F(x, y)) = \sum_{x=1}^{m} \sum_{y=1}^{n} (R[F(x, y)]), \quad (14)$$

where $E_{\max}(F(x, y))$ is the max value of $R[F(x, y)]$, and $E_{total}(F(x, y))$ is the total sum of all the values of $R[F(x, y)]$. In this approach, $E_{total}(F(x, y))$ is adopted. And when we calculated $E_{total}(F(x, y))$, some restrictions were adopted to remove the energies of some noisy lines. Next, by comparing $E_{total}(LA\_image(x, y))$ with $E_{total}(LB\_image(x, y))$, the above question can be easily answered. The corresponding program code scheme is written as follows:

IF $E_{total}(LA\_image(x, y)) > E_{total}(LB\_image(x, y))$
THEN LA_image contains principal lines
ELSE LB_image contains principal lines
END IF

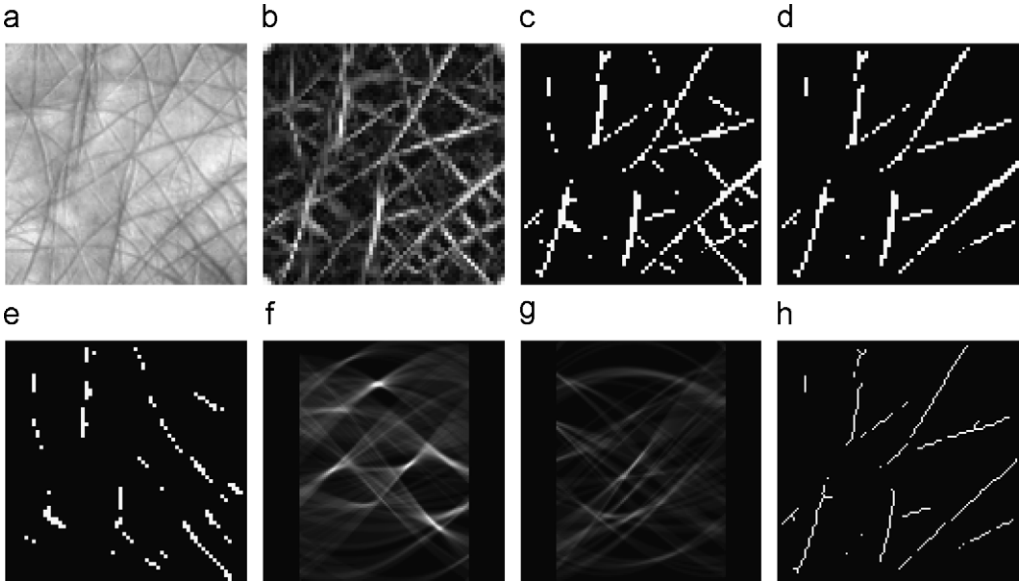

Fig. 3. Images appearing in feature extraction stage. (a) Original image; (b) *Energy_image*; (c) *Lines_image*; (d) *LA_image*; (e) *LB_image*; (f) *R(LA_image)*; (g) *R(LB_image)*; (h) thinning lines of (d).

In the above example, the principal lines are located in *LA_image*. At last, the thinned principal lines are depicted in Fig. 3(h).

3. Palmprint matching

The task of palmprint matching is to calculate the degree of similarity between a test image and a training image. In our method, the similarity measurement is determined by line matching technique. In Palm-Code [1] and Fusion-Code schemes [4], the normalized Hamming distance was used to calculate similarity degree between a test image and a training image, while the Angular distance was adopted in Competitive-Code scheme [11]. However, Hamming distance and Angular distance based on pixel-to-pixel comparison are not suitable for line matching since the line points of the same lines may not be superposed on the palmprints captured from the same palm at a different time. In this section, we devise an algorithm based on pixel-to-area comparison for robust line matching.

Suppose that A is a test image and B is a training image, and the size of A and B is $m \times n$. In A and B, which are all binary images, the value of principal line point is 1. The matching score from A to B is defined as follows:

$$s(A, B) = \left(\sum_{i=1}^{m} \sum_{j=1}^{n} A(i, j) \cap \bar{B}(i, j) \right) \Big/ N_A \tag{15}$$

where "$\cap$" is the logical "AND" operation, N_A is the number of points on detected principal lines in A, and $\bar{B}(i, j)$ is a small area around $B(i, j)$. In our approach, $\bar{B}(i, j)$ is defined as $B(i+1, j)$, $B(i-1, j)$, $B(i, j)$, $B(i, j+1)$, and $B(i, j-1)$. Obviously, the value of $A(i, j) \cap \bar{B}(i, j)$ will be 1 if $A(i, j)$ and at least one point of $\bar{B}(i, j)$ are principal line points simultaneously. Fig. 4 shows the difference between pixel-to-pixel comparison (see Fig. 4(a)) and pixel-to-area comparison (see Fig. 4(b)). The essence of $s(A, B)$ is that A matches with the dilated B (see Fig. 4(c)).

In the same way, the matching score from B to A can also be defined as

$$s(B, A) = \left(\sum_{i=1}^{m} \sum_{j=1}^{n} B(i, j) \cap \bar{A}(i, j) \right) \Big/ N_B. \tag{16}$$

At last, the matching score between A and B is to satisfy:

$$S(A, B) = S(B, A) = \mathrm{Max}(s(A, B), s(B, A)). \tag{17}$$

Theoretically speaking, $S(A, B)$ is between 0 and 1, and the larger the matching score the greater the similarity between A and B. The matching score of a perfect match is 1. From the definition of $S(A, B)$, it can be seen that it is robust for slight translations and slight rotations between two images. That is, the matching score will change little if the translation is not to exceed one pixel and the rotation is not to exceed 3°. However, because of imperfect preprocessing, there might have large translations in practical applications. In order to overcome this problem, we need to vertically and horizontally translate one of feature images and match them again. The ranges of the vertical and horizontal translations are defined from -2 to 2 pixels. The maximum value of $S(A, B)$ obtained from translated matching is considered as the final matching score.

On the other hand, the proposed matching method is also robust for the results of principal lines extraction. As shown in Fig. 5, two feature images were obtained from the same palm, where there are no translations and rotations between them. And one of principal lines could not be extracted in Fig. 5(b). However, the matching score between them is still 1, which can be regarded as a perfect matching.

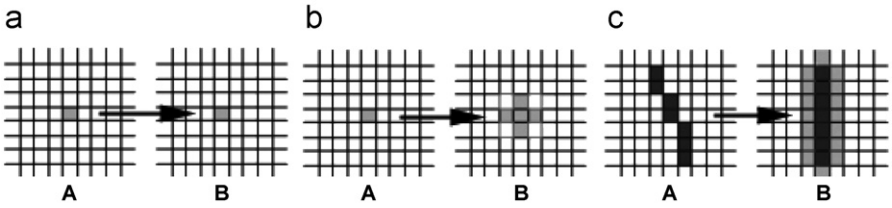

Fig. 4. Pixel-to-pixel comparison and pixel-to-area comparison.

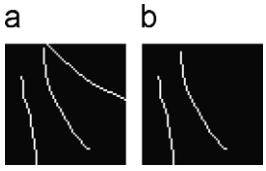

Fig. 5. Principal lines extracted from the same palm, but different images.

4. Experimental results

The proposed approach in this paper was tested in the Hong Kong Polytechnic University (PolyU) Palmprint Database, which is available from website [19]. The PolyU Palmprint Database contains 7752 grayscale images in BMP image format, corresponding to 386 different palms. In this database, around 20 samples from each of these palms were collected in two sessions, where around 10 samples were captured in the first session and the second session, respectively. The average interval between the first and the second collection was two months. The resolution of all the original palmprint images is 384×284 pixels at 75 dpi. Although the resolution is low, the principal lines and the wrinkles are still clear.

Usually, a square region is generally identified as the ROI before feature extraction. Thus, the relevant features are extracted and matched only in this square region. The benefit of this processing is that it can define a coordinate system to align different palmprint images captured from the same palm. Otherwise, the matching result would be unreliable. In this paper, by using the similar preprocessing approach described in literature [1], palmprints were orientated and the ROI, whose size is 128×128, was cropped.

4.1. Results for proposed feature extraction method

Fig. 6 shows two examples of proposed feature extraction method using 14×14 MFRAT described in Section 2. Fig. 6(a) shows a simple palmprint image, which contains clear principal lines and few wrinkles. From Fig. 6(b), it can be seen that the principal lines were perfectly extracted. Even in the case of a complex palmprint images as shown in Fig. 6(c), our method also obtained a satisfying result, which is illustrated in Fig. 6(d).

In the MFRAT, some parameters can be adjusted, which are the size of Z_p^2 determined by p, the number of line directions N, the width of $L(\theta_k)$, W, and the threshold, T, determined by M. The results of feature extraction are generally influenced by these parameters. Here, we changed the values of p and M to analyze the corresponding influence. At first, we adjusted M to extract principal lines using the 14×14 MFRAT ($p = 14$, $N = 12$, and $W = 2$). Fig. 7(a) shows the result extracted from Fig. 3(a) while M was 500, and Fig. 7(b) shows the result while M was 1800. From these two images, it can be concluded that if more lines need to be extracted, we should choose a larger M, otherwise it would be better to adopt a smaller M. Secondly, we conducted two experiments using different p. Fig. 7(c) illustrates the result of the feature extraction method using 7×7 MFRAT described in Section 2 ($p = 7$, $N = 12$, $W = 1$, and $M = 1000$), while Fig. 7(d) depicts the result using 22×22 MFRAT ($p = 22$, $N = 12$, $W = 2$, and $M = 1000$). Compared with Fig. 7(d), it can be found that there are more short lines in Fig. 7(c). In this regard, we can conclude that if there are more short lines or curves with large curvatures to be extracted, a smaller p should be adopted, otherwise a larger p is a better choice.

4.2. Comparison with Gabor filter

Generally speaking, the Gabor filter is also a powerful tool to detect the directional energies of lines. For example, it was often used for fingerprint image enhancement [24]. However, the Gabor filter is not suitable for detecting the directional energies of palm lines. The main reason is that its band limitation restricts its ability to detect the lines with different widths. Yang *et al.* discussed this problem in their fingerprint image enhancement work [24]. They pointed out that the ridge width and valley width often varied in different fingerprint images or in different regions. Thus, applying Gabor filters with a fixed bandwidth often resulted in some artifacts [24]. Similarly, the same situation may occur on detecting palm lines since the width of palm lines is also quite different, especially the ones between principal lines and wrinkles. On the contrary, the MFRAT has no such drawback.

In order to compare their performances, the MFRAT and circular Gabor filters with 12 directions were applied to detect the lines' directional energies of Figs. 3(a) and 6(c), respectively. Here, the circular Gabor filter has the following form:

$$G(x, y, \theta, u, \sigma) = \frac{1}{2\pi\sigma^2} \exp\left\{-\frac{x^2 + y^2}{2\sigma^2}\right\} \exp\{2\pi \mathrm{i}(ux \cos\theta + uy \sin\theta)\}, \quad (18)$$

where $\mathrm{i} = \sqrt{-1}$, u is the frequency of the sinusoidal wave, θ controls the orientation of the function, and σ is the standard deviation of the Gaussian envelope. Figs. 8 and 9 depict the

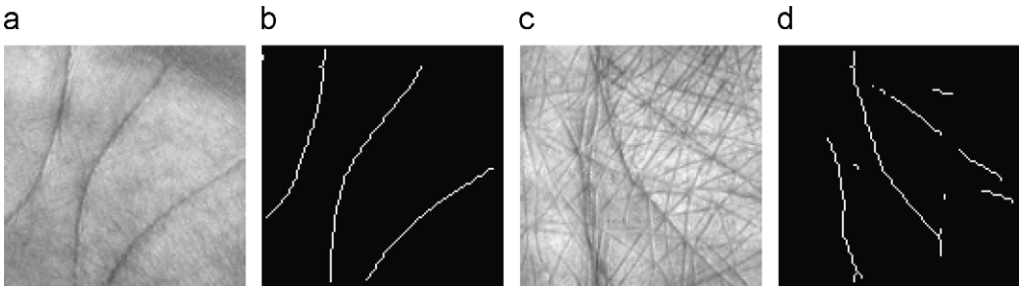

Fig. 6. Extracting principal lines from two different palmprints.

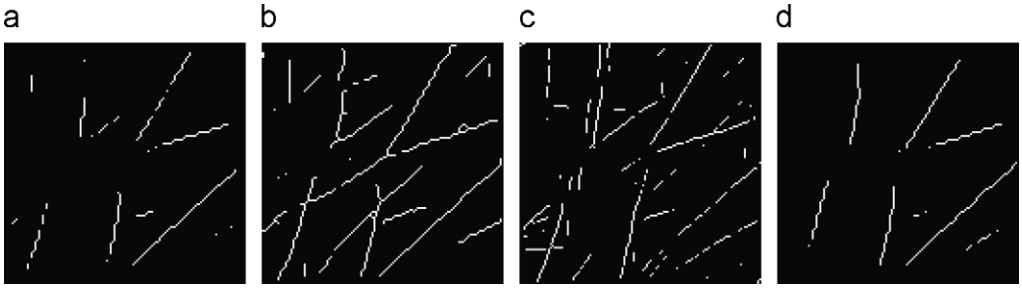

Fig. 7. Extracting principal lines using different parameters. (a) $M=500$, $p=14$, $N=12$, and $W=2$; (b) $M=1800$, $p=14$, $N=12$, and $W=2$; (c) $p=7$, $N=12$, $W=1$, and $M=1000$; (d) $p=22$, $N=12$, $W=2$, and $M=1000$.

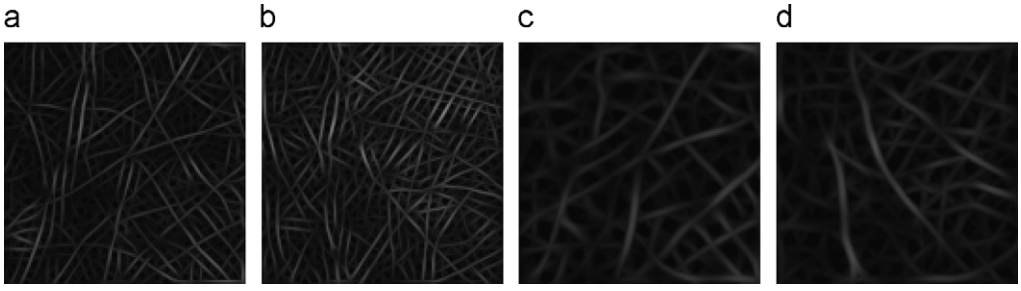

Fig. 8. The directional energies of lines detected from Figs. 3(a) and 6(c) by Gabor filter with different parameters. (a) and (b) $u=0.2$, $\sigma=3.5$, and the size of filter is 20×20; (c) and (d) $u=0.0916$, $\sigma=5.6179$, and the size of filter is 35×35.

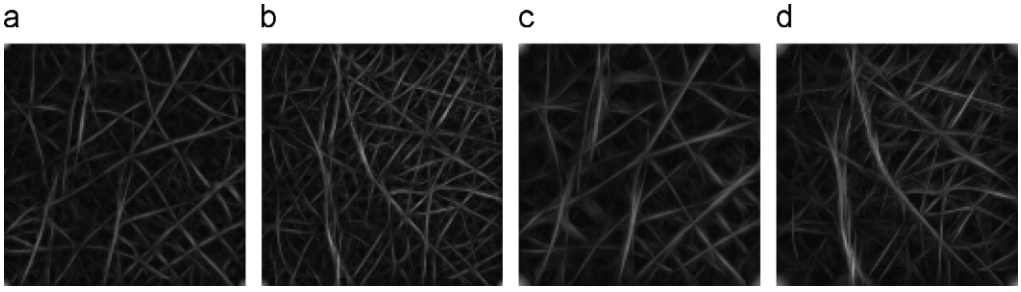

Fig. 9. The directional energies of lines detected from Figs. 3(a) and 6(c) by using 9×9 and 17×17 MFRAT. (a) and (b) $p=9$, $N=12$, and $W=1$; (c) and (d) $p=17$, $N=12$, and $W=1$.

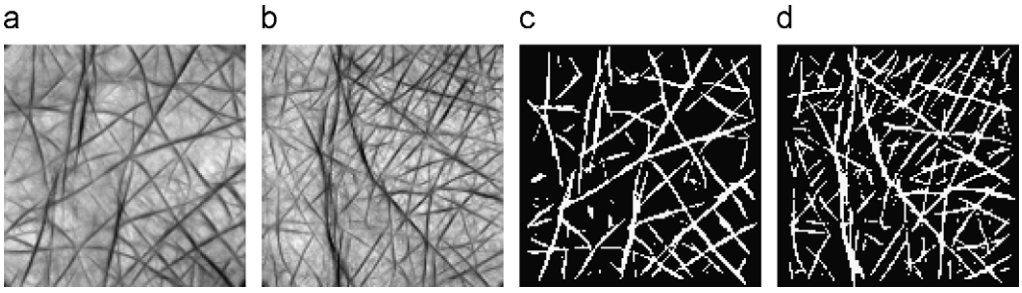

Fig. 10. Enhanced palmprint image and extracted palm lines using 9 × 9 MFRAT. (a) and (b) Enhanced palmprint image; (c) and (d) extracted palm lines from (a) and (b).

corresponding results. It can be found that the performance of Gabor filter is not satisfying (see Fig. 8). For example, given a narrow bandwidth, Gabor filter cannot correctly detect the directional energies of wide lines (see Figs. 8(a) and (b)), and vice versa (see Figs. 8(c) and (d)). In addition, there are some obvious artifacts in Figs. 8(a) and 8(b). On the contrary, the energies of all lines were computed accurately by the MFRAT (see Fig. 9). Moreover, we can use the MFRAT to enhance palmprint image. If we subtract directional energies (Figs. 9(a) and (b)) from original images (Figs. 3(a) and 6(c)), we can get the enhanced images (Figs. 10(a) and (b)), in which all palm lines are more clear and distinct. Particularly, all palm lines can be easily extracted from these enhanced images. Here, suppose that A is an enhanced image, and B is a filtered image by applying a mean filter whose size is about 10×10 to A. The palm lines image, D, is extracted by the following formula:

$$D = B - A - c \times I, \tag{19}$$

where c is a positive integer to control noise, and I is an identity matrix. At last, we obtain the palm lines image after binarizing D. Figs. 10(c) and (d) are the palm lines extracted from Figs. 10(a) and (b), respectively. From this experiment, it can be concluded that the MFRAT is an effective and powerful tool to extract palm lines.

Additionally, another advantage of the MFRAT is its computational efficiency. It runs very fast since only addition operation is involved according to Formula (5). On the contrary, the convolution between one image and Gabor filters involves a mass of multiplication operations. An experiment has been conducted on a PC (the CPU is Pentium 4 (2.4 GHz) and the software platform is Matlab 7.0) to compare their speeds. The execution times of feature extraction using the MFRAT ($p=14$, $W=2$) and Gabor filters (the size is 35×35) are about 410 and 930 ms, respectively.

4.3. Comparison with Liu's and Wu's approaches

Liu et al. and Wu et al. also proposed two different approaches for palmprint recognition, which exploited all palm lines. In Refs. [17] and [18], Liu *et al.* presented a novel wide line detector using an isotropic nonlinear filter. This detector can group pixels whose brightness is similar to the mask center's one into a *weighted mask having similar brightness* (WMSB).

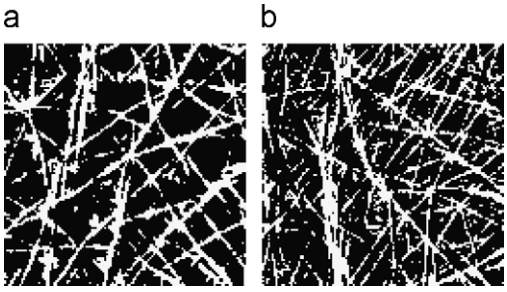

Fig. 11. Palm lines detected from Figs. 3(a) and 6(c) using Liu's approach.

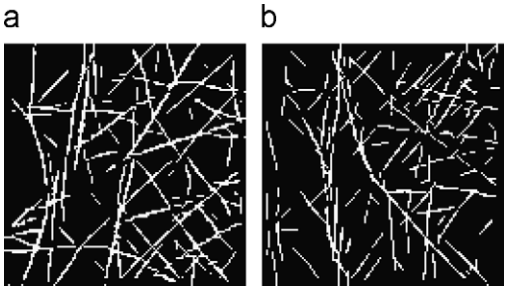

Fig. 12. Palm lines detected from Figs. 3(a) and 6(c) using Wu's approach.

The smaller the WMSB is, the larger the line response will be. In fact, Liu's approach is similar to the SUSAN corner detector to some extent [25], and actually is a segmentation based approach. However, this approach cannot enhance the original image before segmentation. Therefore, it may fail when the palm lines are not clear. And it often incorrectly extracts the small dark patches as a part of palm lines. Moreover, it cannot detect the lines' direction, which is an important feature to distinguish principal lines from wrinkles. Figs. 11(a) and (b) show the palm lines detected from Figs. 3(a) and 6(c) using Liu's approach. It can be seen that its results contain many noises. In Figs. 10(c) and (d), the palm lines can be clearly detected by using our approach since the image was enhanced along the lines' directions during feature extraction stage.

Wu et al. treated palm lines as a kind of roof edge, and extracted them according to the zero-cross points of image's first-order derivative and the magnitude of the edge points' second derivative [15,16]. Therefore, two 1-D Gaussian functions,

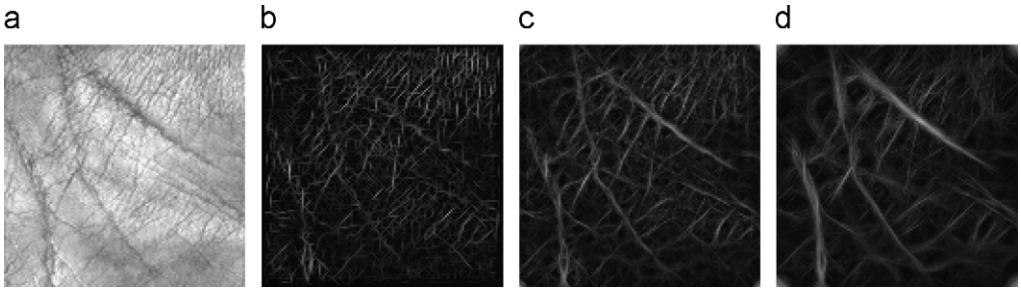

Fig. 13. Comparing Wu's approach with proposed approach. (a) Original palmprint image containing wide principal lines. (b) Magnitude of second derivative detected from (a) by using Wu's approach. (c) Directional energies detected from (a) by using 9×9 MFRAT ($N = 12$ and $W = 1$). (d) Directional energies detected from (a) by using 17×17 MFRAT ($N = 12$, and $W = 1$).

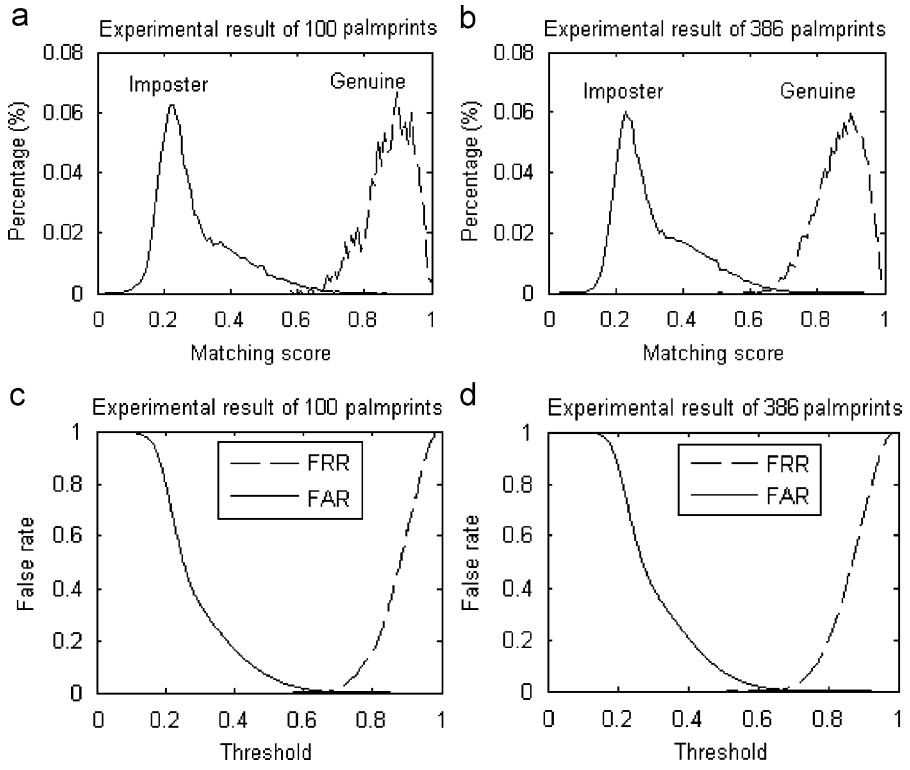

Fig. 14. Experimental results of verification. (a) and (b) Genuine and imposter distributions of matching scores for Databases I and II. (c) and (d) FAR and FRR curves for Databases I and II.

$G_{\sigma s}$ with variance σ_s and $G_{\sigma d}$ with variance σ_d, were used to smooth image and calculate the first- and second-order derivatives of image. Here, σ_s and σ_d were two important parameters to control the smoothness and the width of lines to be detected. And they were determined as 1.8 and 0.5, respectively. However, as the authors have pointed out in Ref. [16], it was impossible to extract all of the lines from various palm prints by using fixed σ_s and σ_d. Thin lines can be detected well by using the selected parameters. Two examples were given in Fig. 12, which depicts the detected lines from Figs. 3(a) and 6(c). However, using the same parameters, their approach may fail to extract those wide lines. Fig. 13(a) is a palmprint image which contains wide principal lines. Fig. 13(b) depicts the magnitude of second derivative detected from Fig. 13(a) by using Wu's approach. Obviously, the principal lines are unclear and difficult to be extracted. The directional energies detected from Fig. 13(a) are shown in Figs. 13(c) and (d), respectively, by using the MFRAT with the two sizes of 9×9 and 17×17. It can be seen that the directional energies of all the lines, both principal lines and wrinkles, were correctly computed. In Ref. [15], the authors used the same method to extract the principal lines for classification. However, some key points, such as potential beginnings of the principal lines, must be detected firstly as prior knowledge before line detection. On the contrary, our approach is independent on image content. In addition, in order to solve rotation problem in palmprint matching stage, Wu's approach aims at rotating the palm lines image a few degrees and then merging all rotated images by using logical "OR" operation so

Table 1
Experimental results near cross-over points (boldface) in Fig. 14

Threshold (R)	FAR (%)	FRR (%)
(a) Results from 100 palmprints (Database I)		
0.571	2.624	0
0.600	1.7037	0.0998
0.650	0.7238	0.3992
0.667	**0.4929**	**0.499**
0.690	0.3024	1.2974
0.750	0.0635	6.487
0.800	9×10^{-3}	15.6687
0.856	1×10^{-3}	37.125
(b) Result from 386 palmprints (Database II)		
0.509	7.0789	0
0.550	4.1695	0.0256
0.600	1.9899	0.1027
0.667	**0.565**	**0.5652**
0.700	0.2865	1.7928
0.750	0.0893	7.3998
0.850	4×10^{-3}	39.748
0.923	6×10^{-5}	78.699

as to construct a dilated image as a training image. However, our proposed matching method can directly solve slight rotations by using pixel-to-area comparison.

4.4. Verification

Verification is a one-to-one comparison against a single stored template, which answers the question of "whether the person is whom he claims to be". In the verification experiments, we set up two databases with different sizes. Database I contains images from first 100 palmprints, and Database II contains all images from 386 palmprints. The aim of setting up two databases is to analyze the discriminability of principal lines in the databases with different sizes. In these two databases, three samples of each palm captured in first session were selected to construct a training set (or a template). Around 10 samples of each palm captured in the second session were taken as the test set.

In experiments, the statistical pairs of FRR and FAR were adopted to evaluate the performance of our approach. To obtain the statistical pairs of FRR and FAR, each of the test images was matched with all of the templates. If the test palmprint image and the template are from the same palm, the matching between them is remarked as a correct matching. Likewise, an incorrect matching can also be defined in a similar manner. Since each template has three palmprint images in the training database, each test image can thus generate three scores. The maximum of them is regarded as a correct matching score at last. Similarly, when a test image matches with another template that comes from a different palm, three incorrect scores can be calculated, and the maximum of them is regarded as an incorrect verification matching score. As a result, for Database I, the number of correct and incorrect matchings are 1002 and 99 198, respectively. And for Database II, the number of correct and incorrect matchings are 3892 and 1 498 420, respectively.

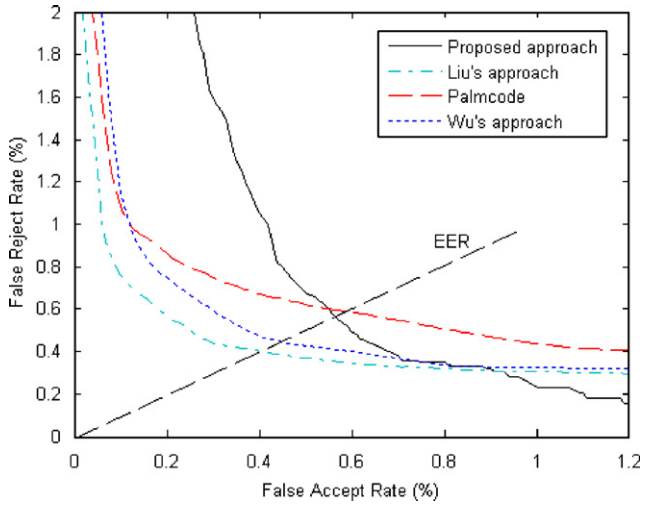

Fig. 15. ROC curves of the proposed approach, Palmcode, Wu's approach, and Liu's approach.

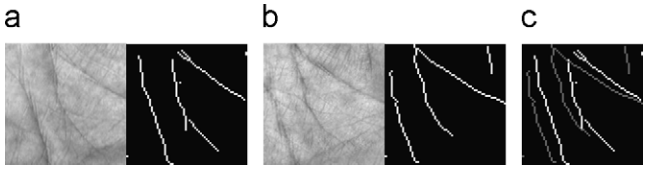

Fig. 16. The principal lines from two people with similar structure, but with dissimilar position.

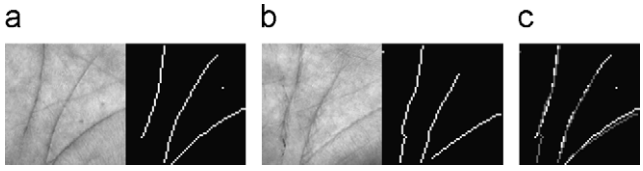

Fig. 17. The principal lines from two people with similar structure and position.

Figs. 14(a) and (b) show the distributions of the genuine and impostor matching scores obtained from two databases, respectively. They are shown that there are two distinct peaks in the distributions of the matching scores. One peak (located around 0.9) corresponds to the genuine matching scores while the other peak (located around 0.2) corresponds to the impostor matching sores. These two peaks are widely separated and the distribution curve of the genuine matching scores intersects very little with that of impostor matching scores. Therefore, it can be concluded that the proposed approach can very effectively discriminate palmprints.

Figs. 14(c) and (d) depict the corresponding FAR and FRR curves for Databases I and II, respectively. In the experiments, assuming that the correlation threshold value is set to R, the experimental results near the cross-over point of the FAR and FRR curves are tabulated in Table 1.

In Fig. 14, it can be easily seen that the matching score curves and FAR&FRR curves, obtained in Databases I and

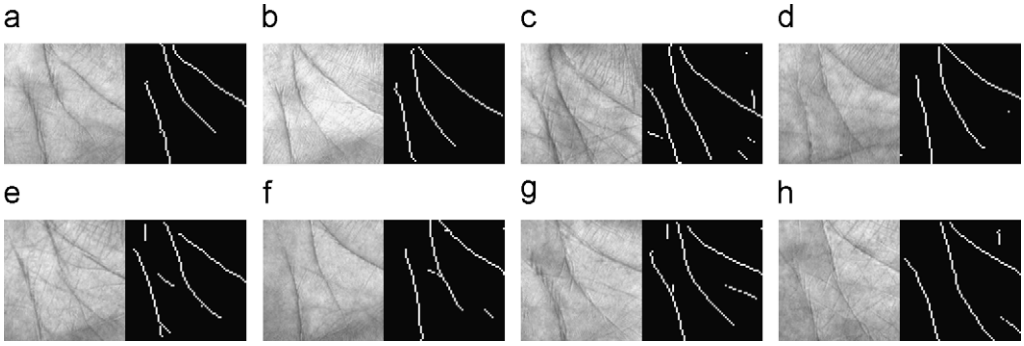

Fig. 18. Eight palmprint images from different people, which have similar principal lines.

Table 2
Matching scores among different palmprint images in Fig. 18

Figs	a	b	c	d	e	f	g	h
a		0.2143	0.2483	0.5310	0.4552	0.4414	0.5216	0.3310
b			**0.6857**	0.3071	0.3000	0.0929	0.1500	0.2000
c				0.1918	0.2767	0.1757	0.2573	0.2988
d					0.4052	**0.7230**	0.5882	0.4641
e						0.3851	0.3711	0.4654
f							0.3243	0.5405
g								0.3720
h								

II, are similar. This demonstrates that the performance of the proposed approach is stable in different size's databases. When the R is set to 0.667, the equal error rates (EER) obtained on Databases I and II, where FAR equals FRR, are about 0.49 and 0.565, respectively. The EER on Database II is obviously larger than that of Database I. A reasonable explanation for this phenomenon is that there is a large probability that a palmprint encounters other palmprints with similar principal lines in large size database.

Further, the results coming from our approach and other approaches, such as Palmcode [1], Wu's approach [16], and Liu's approach [17] were compared. And these approaches were all implemented in Database II by using the same training and test sets. Fig. 15 depicts the corresponding Receiver Operating Characteristic (ROC) curves, which is a plot of false reject rate against false acceptance rate. In this figure, the EERs of Palmcode, Liu's approach, and Wu's approach are 0.59, 0.4, and 0.44, respectively. It can be seen that the EER of our approach is a little better than that of Palmcode, a classical texture based approach. However, the wrinkles may also possess the discriminant power for recognition. Thus, the EERs of Liu's approach and Wu's approach are less than that of the proposed approach.

4.5. Speed

The experiments for the proposed approach were conducted on a personal computer with an Intel Pentium 4 processor (2.4 GHz) and 256 MB RAM configured with Microsoft Windows XP and Matlab 7.0 with image processing toolbox. The execution time for the preprocessing, feature extraction, and matching are 285, 410, and 1.8 ms, respectively. The total execution time is about 0.7 s, which shows that this method is fast enough for real-time verification. In fact, we have not completely optimized the program codes, so it is possible for us to further reduce the computation time.

5. Discussions

In verification experiments, the EER for our approach is even better than that of Palmcode. We can conclude that the discriminability of principal lines is also strong. In the past, many researchers claimed that the discriminability of principal lines was limited due to their similarity among different people. Obviously, this conclusion is not right.

In fact, the similarities of the principal lines among different people include structure similarity and position similarity. For example, the principal lines of Figs. 16(a) and (b) have similar structures, but their positions are dissimilar, as shown in Fig. 16(c). As a result, the matching score between them is only 0.1635, which is a small value. In the past, researchers only paid attention to the structure similarity, but ignored the position dissimilarity of the principal lines among different people. Therefore, they derived an incorrect conclusion about the discriminability of principal lines.

On the other hand, certainly there are a few people whose principal lines may be very similar. For instance, the matching score between two different people may exceed 0.9. Furthermore, in Table 1 even when the threshold is set to 0.923, the value of FAR is still not zero. The principal lines of Figs. 17(a)

and (b) have similar structures and positions (see Fig. 17(c)), thus the matching score between them is very large, which is 0.906.

Fig. 18 illustrates eight palmprint images coming from different people, which have similar principal lines.Table 2 shows the matching scores among them. It can be seen that among all 28 values, only two of them are large, shown in boldface.

6. Conclusions

In this paper, we propose a novel palmprint verification approach based on principal lines, and analyze the discriminability of principal lines. The theoretic analyses and experimental results show that the proposed MFRAT can extract principal lines from complex palmprint images effectively and reliably. And pixel-to-area comparison is robust for slight rotations and translations. From the experimental results of verification, it can be concluded that the discriminability of principal lines is also strong. In the past, many researchers claimed that the discriminability of principal lines was limited. However, they only paid attention to the structure similarity, but ignored the position dissimilarity of principal lines among different people.

Compared to other approaches, our proposed approach only using principal lines may miss other useful features. In the future work, we shall study how to use principal lines, texture and other features to design a multiple features based verification scheme. In this way, a better performance of the PVS can be expected. At the same time, we shall also investigate how to use principal lines to design palmprint classification systems or fast palmprint retrieval schemes.

Acknowledgments

The authors would like to express their sincere thanks to Biometric Research Center at the Hong Kong Polytechnic University for providing us the PolyU Palmprint Database. They would also like to thank Dr Zhenan Sun from Institute of Automation, CAS, China, and Dr Li Liu from Hong Kong Polytechnic University for their kindly help. And the authors are most grateful for the constructive advice and comments from the anonymous reviewers.

This work was supported by the grants of the National Science Foundation of China, Nos. 60472111 and 60705007, the grant from the National Basic Research Program of China (973 Program), No. 2007CB311002, the grants from the National High Technology Research and Development Program of China (863 Program), No. 2007AA01Z167.

References

[1] D. Zhang, A. Kong, J. You, M. Wong, Online palmprint identification, IEEE Trans. Pattern Anal. Mach. Intell. 25 (9) (2003) 1041–1050.

[2] A.K. Jain, L. Hong, R. Bolle, Online fingerprint verification, IEEE Trans. Pattern Anal. Mach. Intell. 19 (4) (1997) 302–314.

[3] L. Ma, T.N. Tan, Y.H. Wang, D.X. Zhang, Personal identification based on iris texture analysis, IEEE Trans. Pattern Anal. Mach. Intell. 25 (12) (2003) 1519–1533.

[4] A. Kong, D. Zhang, M. Kamel, Palmprint identification using feature-level fusion, Pattern Recognition 39 (2006) 478–487.

[5] T. Connie, A.T.B. Jin, M.G.K. On, D.N.C. Ling, An automated palmprint recognition system, Image Vision Comput. 23 (5) (2005) 501–515.

[6] S. Ribaric, I. Fratric, A biometric identification system based on eigenpalm and eigenfinger features, IEEE Trans. Pattern Anal. Mach. Intell. 27 (11) (2005) 1698–1709.

[7] J. Yang, D. Zhang, J.Y. Yang, B. Niu, Globally maximizing locally minimizing: Unsupervised Discriminant Projection with applications to face and palm Biometrics, IEEE Trans. Pattern Anal. Mach. Intell. 29 (4) (2007) 650–664.

[8] L. Shang, D.S. Huang, J.X. Du, C.H. Zheng, Palmprint recognition using FastICA algorithm and radial basis probabilistic neural network, Neurocomputing 69 (13–15) (2006) 1782–1786.

[9] A. Kumar, D. Zhang, Personal authentication using multiple palmprint representation, Pattern Recognition 38 (10) (2005) 1695–1704.

[10] Z.N. Sun, T.N. Tan, Y.H. Wang, S.Z Li, Ordinal palmprint representation for personal identification, in: Proceedings of IEEE International Conference on Computer Vision and Pattern Recognition, 2005, pp. 279–284.

[11] A. Kong, D. Zhang, Competitive coding scheme for palmprint verification, in: Proceedings of the 17th ICPR, vol. 1, 2004, pp. 520–523.

[12] L. Zhang, D. Zhang, Characterization of palmprints by wavelet signatures via directional context modeling, IEEE Trans. Syst. Man Cybern. B. 34 (3) (2004) 1335–1347.

[13] C.C. Han, H.L. Cheng, C.L. Lin, K.C. Fan, Personal authentication using palmprint features, Pattern Recognition 36 (2) (2003) 371–381.

[14] C.L. Lin, T.C. Chuang, K.C. Fan, Palmprint verification using hierarchical decomposition, Pattern Recognition 38 (12) (2005) 2639–2652.

[15] X.Q. Wu, D. Zhang, K.Q. Wang, B. Huang, Palmprint classification using principal lines, Pattern Recognition 37 (10) (2004) 1987–1998.

[16] X.Q. Wu, D. Zhang, K.Q. Wang, Palm line extraction and matching for personal authentication, IEEE Trans. Syst. Man Cybern. A 36 (5) (2006) 978–987.

[17] L. Liu, D. Zhang, A novel palm-line detector, in: Proceedings of the 5th AVBPA, 2005, pp. 563–571.

[18] L. Liu, D. Zhang, J. You, Detecting wide lines using isotropic nonlinear filtering, IEEE Trans. Image Procession 16 (6) (2007) 1584–1595.

[19] PolyU Palmprint Database, ⟨http://www4.comp.polyu.edu.hk/~biometrics/⟩.

[20] J. Radon, Über die bestimmung von funktionen durch ihre integralwerte längs gewisser mannigfaltigkeiten, Berichte Sächsische Akademie der Wissenschafter, Leipzig, Math.-Phys. Kl (69) (1917) 262–267.

[21] A.C. Copeland, G. Ravichandran, M.M. Trivedi, Localized radon transform-based detection of ship wakes in SAR images, IEEE Trans. Geosci. Remote Sensing 33 (1) (1995) 35–45.

[22] F. Matus, J. Flusser, Image representations via a finite radon transform, IEEE Trans. Pattern. Anal. Mach. Intell. 15 (10) (1993) 996–1006.

[23] M.N. Do, M. Vetterli, The finite ridgelet transform for image representation, IEEE Trans. Image Procession 12 (1) (2003) 16–28.

[24] J.W. Yang, L.F. Liu, T.Z. Jiang, A modified Gabor filter design method for fingerprint image enhancement, Pattern Recognition Lett. 24 (12) (2003) 1805–1817.

[25] S.M. Smith, J.M. Brady, SUSAN—A new approach to low level image processing, Int. J. Comput. Vision 23 (1) (1997) 45–78.

About the Author—DE-SHUANG HUANG received the B.Sc. degree in electronic engineering from the Institute of Electronic Engineering, Hefei, China, in 1986, the M.Sc. degree in electronic engineering from the National Defense University of Science and Technology, Changsha, China, in 1989, and the Ph.D. degree in electronic engineering from Xidian University, Xian, China, in 1993. From 1993 to 1997, he was a Postdoctoral Student at the Beijing Institute of Technology, Beijing, China, and the National Key Laboratory of Pattern Recognition, Chinese Academy of Sciences (CAS), Beijing. In 2000, he was a professor, and joined the Institute of Intelligent Machines, CAS, as a member of the Hundred Talents Program of CAS. He had published over 190 papers and,

in 1996, published a book entitled *Systematic Theory of Neural Networks for Pattern Recognition*. His research interests include pattern recognition, machine leaning, bioinformatics, and image processing.

About the Author—WEI JIA received the B.Sc. degree in informatics from Center of China Normal University, Wuhan, China, in 1998, the M.Sc. degree in computer science from Hefei University of Technology, Hefei, China, in 2004. He is currently a Ph.D. student in the Department of Automation at the University of Science and Technology of China. His research interests include palmprint recognition, pattern recognition, and image processing.

About the author—DAVID ZHANG graduated in computer science from Peking University. He received his M.Sc. in computer science in 1982 and his Ph.d. in 1985 from the Harbin Institute of Technology (HIT). From 1986 to 1988 he was a Postdoctoral Fellow at Tsinghua University and then an Associate Professor at the Academia Sinica, Beijing. In 1994 he received his second Ph.D. in electrical and computer engineering from the University of Waterloo, Ont., Canada. Currently, he is a Chair Professor at the Hong Kong Polytechnic University where he is the Founding Director of the Biometrics Technology Centre (UGC/CRC) supported by the Hong Kong SAR Government. He also serves as Adjunct Professor in Tsinghua University, Shanghai Jiao Tong University, Beihang University, Harbin Institute of Technology, and the University of Waterloo. He is the Founder and Editor-in-Chief, International Journal of Image and Graphics (IJIG); Book Editor, Springer International Series on Biometrics (KISB); Organizer, the International Conference on Biometrics Authentication (ICBA); Associate Editor of more than 10 international journals including IEEE Trans on SMC-A/SMC-C/Pattern Recognition; Technical Committee Chair of IEEE CIS, and the author of more than 10 books and 160 journal papers. Professor Zhang is a Croucher Senior Research Fellow, Distinguished Speaker of the IEEE Computer Society, and a Fellow of the International Association of Pattern Recognition (IAPR).